Kinetic Analysis of *Escherichia coli* 2-C-Methyl-D-erythritol-4-phosphate Cytidyltransferase, Wild Type and Mutants, Reveals Roles of Active Site Amino Acids†

Stéphane B. Richard,‡ Antonietta M. Lillo,§ Charles N. Tetzlaff,§ Marianne E. Bowman,‡ Joseph P. Noel,‡ and David E. Cane*,§

Structural Biology Laboratory, The Salk Institute for Biological Studies, 10010 North Torrey Pines Road, La Jolla, California 92037, and Department of Chemistry, Box H, Brown University, Providence, Rhode Island 02912-9108

Received June 18, 2004; Revised Manuscript Received July 20, 2004

ABSTRACT: *Escherichia coli* 2-C-methyl-D-erythritol-4-phosphate cytidyltransferase (YgbP or IspD) catalyzes the conversion of 2-C-methyl-D-erythritol 4-phosphate (MEP) and cytidine triphosphate (CTP) to 4-diphosphocytidyl-2-C-methylerythritol (CDPME). Pulse chase experiments established that the reaction involves an ordered sequential mechanism with mandatory initial binding of CTP. On the basis of analysis of the previously reported crystal structures of apo-YgbP as well as YgbP complexed with both CTP·Mg^{2+} and CDPME·Mg^{2+} [Richard, S. B., Bowman, M. E., Kwiatkowski, W., Kang, I., Chow, C., Lillo, A. M., Cane, D. E., and Noel, J. P. (2001) *Nat. Struct. Biol. 8*, 641−648], a group of active site residues were selected for site-directed mutagenesis and steady-state kinetic analysis. Both Lys27 and Lys213 were shown to be essential to catalytic activity, consistent with their proposed role in stabilization of a pentacoordinate phosphate transition state resulting from in-line attack of the MEP phosphate on the α-phosphate of CTP. In addition, Thr140, Arg109, Asp106, and Thr165 were all shown to play critical roles in the binding and proper orientation of the MEP substrate.

The mevalonate-independent pathway of isoprenoid biosynthesis, also known as the methylerythritol phosphate (MEP)[1] pathway, is utilized by a wide variety of bacteria, including many human pathogens, as well as various species of streptomycetes, mosses and liverworts, marine diatoms, and higher plants (*1*−*7*) (Scheme 1). Several of these organisms utilize both the classical mevalonate and the MEP pathway, while others use only the MEP pathway for the biosynthesis of the fundamental isoprenoid building blocks isopentenyl diphosphate (IPP, **9**) and dimethylallyl diphosphate (DMAPP, **10**).

The MEP pathway has proven to be a rich source of novel biochemistry. The first committed biochemical step, which gives the pathway its name, is the NADPH-dependent reductive rearrangement of 1-deoxy-D-xylulose 5-phosphate (dXP, **3**) to 2-C-methyl-D-erythritol 4-phosphate (MEP, **4**) catalyzed by the reductoisomerase (DXR or IspC) (*8*). dXP itself is formed by the thiamin diphosphate (TPP)-dependent condensation of pyruvate (**1**) and D-glyceraldehyde 3-phosphate (**2**), catalyzed by dXP synthase (DXS) (*9*, *10*). Interestingly, dXP has also been shown to be a precursor in *Escherichia coli* of both thiamin diphosphate (*11*, *12*) and pyridoxol phosphate (*13*, *14*). MEP undergoes CTP-dependent conversion to 4-(cytidine-5′-diphospho)-2-C-methyl-D-erythritol (CDPME, **5**) catalyzed by MEP cytidyltransferase (also known as CDPME synthetase, designated YgbP or IspD) (*15*, *16*). The 2-hydroxyl group of **5** is phosphorylated by CDPME kinase (YchB) to produce **6** (*17*, *18*), which is then cyclized to the structurally novel 2-C-methyl-D-erythritol-2,4-cyclodiphosphate (**7**) with displacement of cytidine 5′-monophosphate (*19*, *20*). The cyclodiphosphate **7** undergoes an intriguing reductive ring opening to give 1-hydroxy-2-methyl-2(*E*)-butenyl-4-diphosphate (**8**), catalyzed by GcpE (IspG) (*21*−*23*). Finally, LytB (IspH) reduces **8** to a 4:1 mixture of IPP (**9**) and DMAPP (**10**) (*24*−*26*). Both IspG and IspH have been shown to harbor $[4Fe\text{-}4S]^{2+}$ clusters and to require auxiliary electron transport proteins as shuttles for their reducing equivalents (*27*, *28*).

The antibiotic and antimalarial effects of the DXR inhibitor fosmidomycin (*29*) and the immunogenicity of **8** (*30*) suggest that the MEP pathway should be an attractive target for innovative antibacterial, antiparasitic (*31*), and immunomodulatory agents. The inhibition of the MEP pathway in plants might also be the basis for the development of novel herbicides, while the upregulation of the pathway could facilitate the enhanced production of genetically engineered agricul-

† This research was supported by NIH Grants GM30301 (D.E.C.) and AI51438 (J.P.N.).

* To whom correspondence should be addressed. E-mail: david_cane@brown.edu.

‡ The Salk Institute for Biological Studies.

§ Brown University.

[1] Abbreviations: CDPME, 4-(cytidine-5′-diphospho)-2-C-methyl-D-erythritol; CTP, cytidine 5′-triphosphate; DMAPP, dimethylallyl diphosphate; dXP, 1-deoxy-D-xylulose 5-phosphate; DXR, dXP reductoisomerase (or IspC); DXS, dXP synthase; IPP, isopentenyl diphosphate; IPTG, isopropyl thio-D-galactopyranoside; LB, Luria-Bertani; MEP, 2-C-methyl-D-erythritol 4-phosphate; MWCO, molecular weight cutoff; PCR, polymerase chain reaction; SDS−PAGE, sodium dodecyl sulfate−polyacrylamide gel electrophoresis; TB, Terrific Broth; TFA, trifluoroacetic acid; TLC, thin-layer chromatography; TPP, thiamin diphosphate; Tris, tris(hydroxymethyl)aminomethane; wt, wild-type; YgbP, MEP cytidyltransferase (IspD).

10.1021/bi0487241 CCC: $27.50
Published on Web 08/28/2004

Scheme 1: Mevalonate-Independent Biosynthesis of IPP and DMAPP

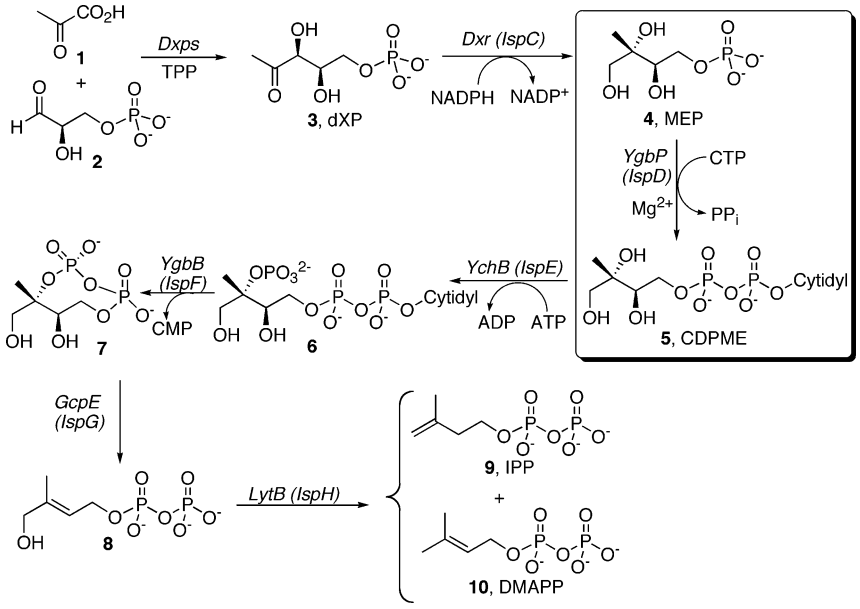

tural products. Genetic manipulation of the enzymes of the MEP pathway might also lead to the biotechnological production of commercially important isoprenoids such as carotenoids.

The identification of all the enzymes and intermediates of the MEP pathway has opened the way to the detailed characterization of the mechanism of each step. For example, the steady-state kinetic properties of wild-type YgbP from *E. coli* (*15*, *32*, *33*) and from *Streptomyces coelicolor* (*33*) have been previously reported, and erythritol 4-phosphate, the 2-desmethyl analogue of MEP, has been shown to inhibit YgbP (*32*, *34*). We have recently reported high-resolution crystal structures of *E. coli* YgbP in its apo form (1.55 Å) as well as with bound CTP·Mg^{2+} (1.50 Å) and with bound CDPME·Mg^{2+} (1.82 Å) (*35*). A 2.40 Å structure of apo *E. coli* YgbP has subsequently been reported by Kemp *et al.* (*36*), and researchers at Structural Genomix have also recently deposited the coordinates for the *Neisseria gonorrhea* protein in the Protein Data Bank.[2] No structural data for YgbP complexed with MEP are available.

E. coli YgbP is a homodimer with each subunit related by a crystallographic 2-fold axis (*35*). In both of the bound structures, the substrate CTP and the product CDPME are each surrounded by a glycine-rich loop encompassing residues 13−20 (Figure 1). Gly82, Asp83, Arg85, and Ser88 are within hydrogen bond or ionic interaction distance of the cytidine moiety. Ala107 is positioned to contribute to the binding of the ribose moiety, while both Lys27 and Lys213 apparently interact with both the α- and *β*-phosphates of CDPME. YgbP residues Asp106, Arg109, Thr163, and Thr165, as well as Thr140′ and Arg157′ contributed by the paired subunit of the homodimer, are close enough to the MEP-derived portion of CDPME to interact directly, suggesting that they also interact with the substrate MEP during the cytidyltransferase reaction.

The structures of YgbP in complex with CTP·Mg^{2+} and with CDPME·Mg^{2+} are consistent with a proposed in-line, associative mechanism involving a pentacoordinate transition

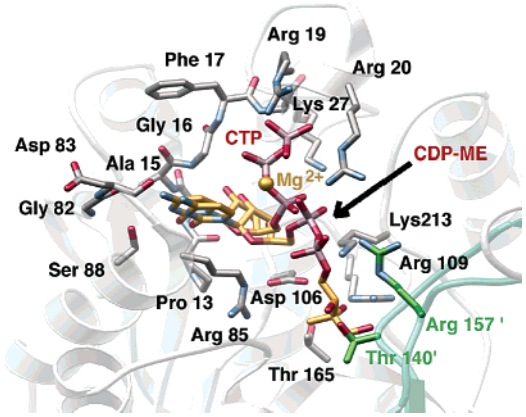

FIGURE 1: CDPME molecule from the YgbP·CDPME complex superimposed with the partial structure of the YgbP·CTP complex, showing interactions with active site residues and the relative positions of the substrate and product. Thr140′ and Arg157′ are contributed by the second subunit of the YgbP dimer.

state or intermediate that would result from nucleophilic attack of the MEP phosphate on the α-phosphate of CTP (Figure 2).[3] In the YgbP−CDPME complex, Lys213 and Lys27 are both involved in an ionic interaction with the α-phosphate of CDPME. Similar interactions are evident in the YgbP−CTP structure. The positively charged side chains of Lys27 and Lys213 could, in principle, stabilize the developing negative charge on the α-phosphate in the proposed pentacoordinate intermediate or transition state. Furthermore, the distance of ∼2.3−2.5 Å between the *β*-phosphate oxygen atoms of CDPME, which is derived from MEP, and the side chain conformation of Lys213 in the YgbP·CTP complex, suggests that this amino acid might also interact with MEP through an H-bond. Preliminary studies using site-directed mutagenesis had indicated that the activities of the YgbP K27A, K27S, and K213S mutants are indeed severely compromised (*35*). We now report the results of systematic steady-state kinetic analysis of a series of active

[2] *N. gonorrhea* YgbP (PDB entries 1GVW and 1GVZ).

[3] The apparent in-line geometry is also consistent with an alternative, dissociative mechanism for P−O bond formation.

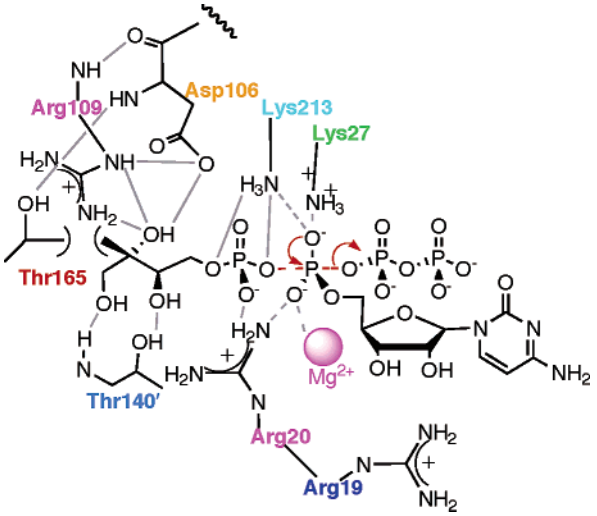

FIGURE 2: Proposed role of active site amino acids in binding of the putative pentacoordinate phosphate intermediate or transition state for the MEP cytidyltransferase reaction. Dashed lines represent ionic interactions, and solid gray lines represent H-bonds.

site mutants of YgbP that elucidate the role of key active residues. We also describe pulse−chase experiments that establish the order of binding of the substrates of the enzyme-catalyzed reaction.

EXPERIMENTAL PROCEDURES

Materials and General Methods. The pHIS8-*ygbP* constructs for both wt and mutants, prepared according to a published procedure (*35*), are derivatives of the pHIS8 vector (*37*), which places a His_8 tag at the N-terminus of the recombinant protein. The wt and mutant constructs were used to transform the *E. coli* BL21(DE3) (Stratagene) expression host according to the vendor's instructions. A GS363 Bio-Rad phosphorimaging system was used for the YgbP assay. ^{1}H NMR (300 MHz) utilized a Bruker Avance AM 300 spectrometer. CTP, Tris-HCl, and all inorganic salts were purchased from Sigma. HCl was obtained from Fluka, and solvents were purchased from Mallinckrodt. Isopropyl thio-D-galactopyranoside (IPTG) was from Gibco. [2-^{14}C]Pyruvate (15.0, 15.8, or 17.5 mCi/mmol) was purchased from New England Nuclear (NEN), and [2-^{14}C]CTP (55 mCi/mmol, 0.1 mCi/mL) was from Moravek Biochemicals. Buffers and gels for SDS−PAGE were prepared according to published procedures (*38*). Nickel chelating columns were purchased from Novagen (Ni−NTA) or Pharmacia (Hitrap Chelating Column). Thrombin (human plasma) was purchased from Sigma, and inorganic pyrophosphatase was from ICN Biochemicals. Benzamidine affinity columns (Benzamidine Sepharose 6B) were obtained from Pharmacia. Dialysis tubes (Spectra/Por membrane, MWCO of 6000−8000) were purchased from Spectrum Medical Industries. Centriprep YM-30 concentrators (Millipore) were used to concentrate 7−15 mL protein solutions. UltraFree-MC (MWCO of 5000) concentrators (Millipore) were used to concentrate 100−500 μL protein solutions. Protein concentrations were determined by the Bradford method (*39*) using bovine serum albumin (Sigma) as a calibration standard. Bradford reagent was purchased from Sigma. Luria-Bertani (LB) medium was prepared according to the standard recipe (*38*). All the components of the culture media were obtained from Difco. *S. coelicolor* Dxps2 (DXS) and *E. coli* DXR were prepared as previously described (*33*). The ammonium salt of MEP was prepared enzymatically from pyruvate and glyceraldehyde 3-phosphate and purified as previously described (*35*). Stock solutions of MEP were prepared in water, and the concentration was determined by ^{1}H NMR, using acetone as an internal standard. Polygram SIL N-HR plates were purchased from Macherey & Nagel. Cellulose $F_{254+366}$ TLC plates (100 μm) were from Merck. The Insight II software package (Accelrys) and the program O (*40*) were used to visualize the PDB files corresponding to the crystal structure of YgbP·CTP (PDB entry 1I52) and YgbP·CDPME (PDB entry 1INJ). Figure 1 was generated using MOLSCRIPT (*41*) and rendered with POV-RAY (http://www.povray.org). Molecular Analyst software was part of the Bio-Rad GS363 phosphorimaging system.

Expression of wt ygbP and Mutants. Saturated seed cultures of *E. coli* BL21(DE3) (5 mL), harboring wt or mutant pHIS8-*ygbP*, were used to inoculate fresh TB medium (500 mL). At an optical density (OD) of 0.7 (A_{600}), the transformants were induced with 0.5 mM IPTG and allowed to grow for an additional 4 h at 37 °C. A 500 μL aliquot of each culture was lysed and analyzed by SDS−PAGE. YgbP was expressed in each culture and accounted for ∼70% of the total protein. The cells were harvested, stored at −80 °C for 2 h, thawed, resuspended in 35 mL of a solution of lysis buffer [50 mM Tris-HCl (pH 7.8), 5 mM $MgCl_2$, 10% glycerol, 500 mM NaCl, 27 mM β-mercaptoethanol, and 20 mM imidazole], and then disrupted by sonication (7 × 3 min burst, 40 MHz, 50% duty cycle). The cell lysates were centrifuged at 4700*g* for 1 h and the supernatants stored at −80 °C.

Enzymatic Preparation of [2-^{14}C]MEP. [2-^{14}C]MEP was prepared by the method previously described (*35*). A solution containing 3.5 μmol of [2-^{14}C]pyruvate (350 μL, 15.8 μCi/μmol), 9 μmol of racemic glyceraldehyde 3-phosphate, 4.5 μmol of NADPH, 60 μg of *S. coelicolor* Dxps2, 75 μg of *E. coli* DXR, 0.7 μmol of TPP, 1.7 μmol of $MnCl_2$, 0.7 μmol of DTT, and 7 μmol of Tris-HCl (pH 8) was incubated at 30 °C for 8 h. Enzymes were then removed by ultrafiltration, and the resultant filtrate was analyzed by TLC (cellulose plates, 45:5:0.5 CH_3CN/H_2O/TFA mixture). The remaining solution (6.5 mM [2-^{14}C]MEP) was combined with an appropriate amount of unlabeled ammonium MEP (*35*) to give the stock solution utilized for assay of YgbP activity.

Assay of Crude E. coli Lysates for MEP Cytidyltransferase Activity. Crude lysates of *E. coli* BL21(DE3) containing overexpressed wild type or mutant YgbP were assayed for MEP cytidyltransferase activity according to a previously described protocol (*15*). This preliminary test allowed selection of those mutants having a detectable activity and therefore worth further purification. Assay mixtures contained [2-^{14}C]MEP (217 nmol, 0.13 nCi/nmol), CTP (81.3 nmol), Tris-HCl (400 nmol), $MgCl_2$ (40 nmol), NaOH (79 nmol), and YgbP (crude cell-free lysate containing wt or mutant protein, 1.0 μg) (final volume of 5 μL). CTP stock solutions were prepared by dissolving CTP disodium salt (Sigma) in buffered solutions containing Tris-HCl and $MgCl_2$ at the same concentrations as in the enzymatic assay mixture. The resulting solutions were brought to pH 6.5 using concentrated aqueous NaOH. Assay mixtures were incubated at 23 °C. After 1 and 15 h, a 1 μL aliquot of each mixture was

quenched and analyzed by thin-layer chromatography (TLC) (*15*). Before the samples were loaded, the baseline of the TLC plates was acidified with 1 μL of 2 N HCl to denature the enzyme in the sample upon loading. [2-^{14}C]CDPME was visualized and quantitated by phosphorimaging (12 h exposure). The intensities of the individual CDPME spots were corrected by subtraction of background intensities at the same TLC R_f, using a blank reaction mixture lacking YgbP. Serially diluted [2-^{14}C]MEP solutions with a known concentration were applied to the top of the TLC plate after elution and used as calibration standards.

His Tag Removal and Purification of ygbP wt and Mutants. Ni−NTA resin was mixed with binding buffer (lysis buffer with 10 mM β-mercaptoethanol and 10 mM imidazole) in a 1:4 (v:v) ratio. The resulting suspension (20 mL) was mixed with each crude lysate containing YgbP (wt or mutant, 15 mL). After gentle agitation (200 rpm) for 1 h at 4 °C, each suspension was transferred to an empty column (10 cm × 2 cm) and each column drained. The equilibrated affinity columns were washed with 32 mL of washing buffer (binding buffer with 60 mM imidazole) and eluted with 8 mL of elution buffer (binding buffer with 250 mM imidazole). $CaCl_2$ (2.5 mM) and thrombin (30 units) were added to each eluate before each was transferred to dialysis tubes. Protein solutions (9 × 7 mL), eluted from the Ni−NTA resin, were allowed to equilibrate against 4 L of dialysis buffer (binding buffer with 200 mM NaCl) for 24 h at 4 °C. These conditions allowed the thrombin to cleave each protein from its His tag. The resulting protein solutions were kept at −80 °C for 48 h, thawed, and mixed with dialysis buffer in a 1:1 ratio. To remove the cleaved His tag, each thrombin-treated protein solution was remixed with a suspension of Ni−NTA resin in 18 mL of dialysis buffer, and the resultant slurry was equilibrated as described above. The His tag-free protein solutions were drained from the resin suspensions directly into thrombin-affinity benzamidine columns (4 mL) previously equilibrated with dialysis buffer. The thrombin-free flow-through containing purified YgbP (8 mL) was collected, and the residual protein trapped by the benzamidine resin was retrieved by washing the column with 2 mL of dialysis buffer. The final protein solutions were analyzed by SDS−PAGE. After staining and digitization, the intensity of the band corresponding to wt or mutant ygbP in each lane was quantified by Molecular Analyst Software as a percentage of the total intensity in the same lane. The YgbP protein solutions were concentrated ∼50-fold and divided into 10 × 15 μL portions before storage at −80 °C. Each aliquot was used for only one kinetic experiment to eliminate multiple cycles of freezing and thawing.

Steady-State Kinetic Analysis of wt and Mutant YgbP. YgbP assay mixtures contained Tris-HCl (398 nmol), $MgCl_2$ (40 nmol), NaOH (79 nmol), and inorganic pyrophosphatase (0.7 unit, to avoid the inhibitory effect of inorganic pyrophosphate) in a total volume of 5 μL. When MEP was the variable substrate (nine different concentrations, from 0.1 to 112 mM), CTP was fixed at concentrations of $\sim 10K_m^{CTP}$ (7−70 mM). When CTP was the variable substrate (nine different concentrations, from 0.2 to 82 mM), [2-^{14}C]MEP was fixed at concentrations of $\sim 10K_m^{MEP}$ (3−130 mM, 0.3−0.9 nCi/nmol). Each reaction was initiated by addition of YgbP. The concentration of the enzyme was such that no more than 10% of the initial substrate was consumed in 12 min. After 6 and 12 min at 23 °C, a 1 μL aliquot of each reaction mixture was quenched as described above and separated by TLC (*15*). The formation of [2-^{14}C]CDPME was quantitated by phosphorimaging, as described above. After elimination of any obvious experimental outliers (observed ≥ 1.5−2 × predicted), seven to nine data points for the rate of formation of CDPME as a function of the concentration of MEP or CTP were fit directly to the appropriate form of the Michaelis−Menten equation (eq 1 or 2) by nonlinear least-squares regression using Kaleidagraph software, giving an average R^2 value of 0.993. Upon finding the optimal experimental conditions, we repeated kinetic assays for each protein several times, to verify the reproducibility of the data.

Pulse−Chase Experiments with wt YgbP. For the MEP pulse−chase experiment, a solution containing 1 nmol of [2-^{14}C]MEP was added to an Eppendorf tube and then concentrated to dryness. A solution of wt YgbP (1 μL, 1 mM, 17.9 mg/mL) was then added to the dry substrate and the mixture allowed to stand at room temperature for 15 min, giving a final concentration of 1 mM MEP ($\sim 3K_m^{MEP}$). To this solution was then added 300 μL of the chase solution which consisted of 10 mM MEP, 10 mM CTP, inorganic pyrophosphatase (4.48 units), Tris (100 mM), $MgCl_2$ (10 mM), and DTT (2 mM) at pH 8, corresponding to a net 3000-fold dilution of the original MEP (*42*). Aliquots (25 μL) were removed every 5 s for 50 s and added to 20 μL of TFA to quench the reaction. The quench solutions were then concentrated via a Speedvac and spotted onto TLC for development and phosphorimaging. Control experiments used unlabeled MEP for the pulse followed by [2-^{14}C]MEP with unlabeled CTP for the chase. Concentrations of MEP and CTP greater than 10 mM were not used due to the K_I of 19.6 mM for substrate inhibition by CTP. The complementary pulse−chase experiment used a pulse of 2.0 mM [2-^{14}C]-CTP ($\sim 3K_m^{CTP}$) and 2.2 mM YgbP, with the same chase solution as for experiments with MEP. The corresponding control experiment utilized unlabeled CTP in the pulse and [2-^{14}C]CTP and MEP in the chase.

RESULTS

Pulse−Chase Determination of the Order of Substrate Binding. Although crystal structures could be obtained for YgbP with one of the bound substrates, CTP in complex with Mg^{2+}, or with bound product, CDPME·Mg^{2+}, all attempts to obtain crystals carrying bound MEP have so far been unsuccessful. The possibility that YgbP protein might not bind MEP in the absence of the cosubstrate CTP was recognized. To test this model directly, we carried out complementary pulse−chase (isotope trapping) experiments in which YgbP was separately premixed with a stoichiometric amount of each labeled substrate, [2-^{14}C]MEP or [2-^{14}C]CTP (the pulse), followed by addition of a chase solution consisting of a 3000-fold excess of a mixture of unlabeled MEP and CTP (*42*). Aliquots of the resulting incubation mixture were withdrawn at 5 s intervals for up to 50 s, quenched in TFA, and analyzed by TLC phosphorimaging. Control experiments utilized unlabeled substrate in the pulse and prediluted, labeled substrate in the chase. The results, illustrated in Figure 3, clearly show that when [2-^{14}C]CTP was used in the pulse, the bulk (>70%) of the isotopically labeled nucleotide could be efficiently trapped on the enzyme

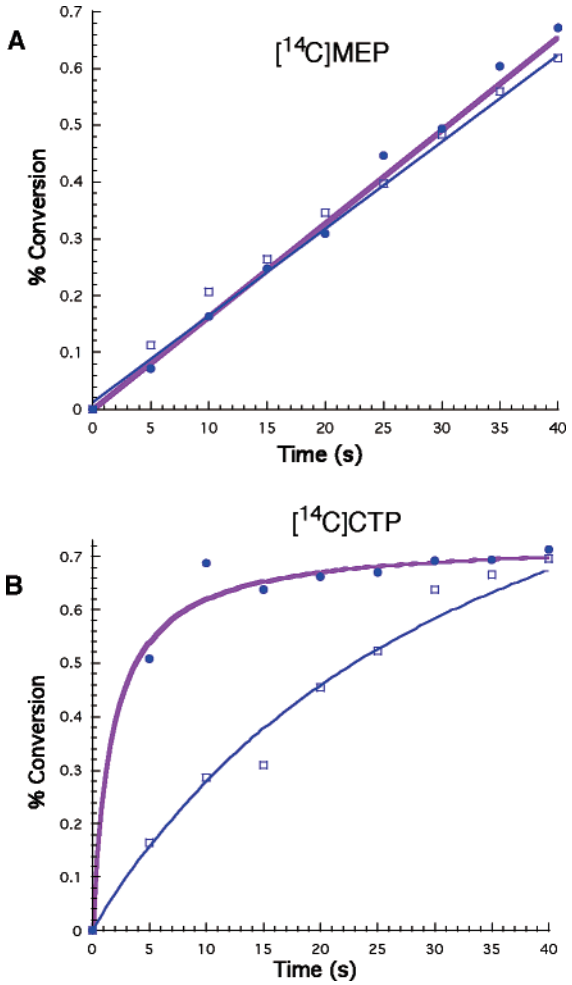

FIGURE 3: Pulse−chase analysis of the YgbP reaction (see Experimental Procedures for details). Time course of formation of [^{14}C]CDPME, plotted as the percent conversion of the ^{14}C-labeled substrate. (A) Pulse with 1 mM [2-^{14}C]MEP (●) and control incubation with [2-^{14}C]MEP in the chase solution (□). (B) Pulse with 2 mM [2-^{14}C]CTP (●) and control incubation with [2-^{14}C]-CTP in the chase solution (□).

and converted to product [^{14}C]CDPME upon addition of the chase solution. (No attempt was made to increase the fraction of trapped CTP by increasing the concentration of MEP in the chase.) By contrast, [2-^{14}C]MEP completely equilibrated with the chase solution before conversion to CDPME. These results are consistent with an ordered, sequential mechanism with mandatory initial binding of CTP.

Assay of the Crude Cell Extracts of wt YgbP and Mutants. Although a significant proportion of recombinant YgbP T165V protein, and the various D106 mutant proteins, were obtained as inclusion bodies, ~60% of the each mutant protein was found in the supernatant, which was more than sufficient for purification and kinetic assay. Cytidyltransferase activity was not detected for the crude cell-free extracts of ygbP mutants D106A, D106N, K213S, K27A, and T165V under conditions which could have detected a decrease in k_{cat} of as much as a factor of 10^4 compared to that of wt YgbP. These mutants were therefore judged to be inactive and were not further purified. The lack of activity of the K27A and K213S mutants was consistent with preliminary results reported previously (*35*). The YgbP K27S mutant retained measurable, albeit significantly reduced, YgbP activity.

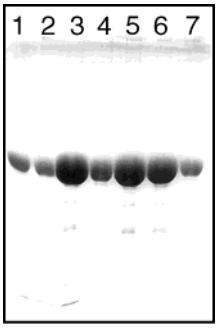

FIGURE 4: SDS−PAGE of purified, recombinant, His tag-free *E. coli* wt YgbP and mutants. The purity of each protein was determined to be ≥95%: lane 1, wt; lane 2, R19A; lane 3, D106E; lane 4, K27S; lane 5, R20K; lane 6, R20A; and lane 7, R19K.

Purification of wt YgbP and Mutants. Nickel affinity chromatography purification followed by thrombin-catalyzed cleavage of the N-terminal His_8 tag afforded ~150 μL of each active mutant protein that was >95% pure as judged by SDS−PAGE (Figure 4). Since each mutant YgbP protein was expressed and purified under identical conditions, the yield of each mutant protein roughly reflected the relative efficiency of expression of the soluble recombinant protein. The most efficiently expressed soluble protein was YgbP mutant D106E (final concentration of 32 mg/mL). The relative expression efficiencies of the other recombinant proteins compared to that of D106E were R20K (77%), R20A (56%), K27S (28%), wt (21%), R19K (18%), and R19A (11%).

Steady-State Kinetic Analysis. The calculated values of k_{cat}^{MEP}, K_m^{MEP}, and k_{cat}/K_m^{MEP} for each YgbP mutant are summarized in Table 1 [average R^2 of 0.993 for fitting to the standard Michaelis−Menten expression (eq 1)]. Since CTP showed marked substrate inhibition, resulting in poor fits to eq 1 when CTP was the varied substrate, the data from the latter sets of experiments were fit to eq 2 which contains a K_i term to account for substrate inhibition (*43*) (average $R^2 = 0.985$). The corresponding values of k_{cat}^{CTP}, K_m^{CTP}, k_{cat}/K_m^{CTP}, and K_i^{CTP} are given in Table 1, and the relative values of k_{cat} are compared graphically in Figure 5.

$$v = V_{max}[S]/([S] + K_m) \quad (1)$$

$$v = V_{max}[S]/([S] + K_m + [S]^2/K_i) \quad (2)$$

$$^{Calc}k_{cat}^{MEP} = {}^{app}k_{cat}^{MEP}(1 + K_m^{CTP}/[CTP] + [CTP]/K_i^{CTP}) \quad (3)$$

$$^{Calc}k_{cat}^{CTP} = {}^{app}k_{cat}^{CTP}(K_m^{MEP} + [MEP])/[MEP] \quad (4)$$

When MEP was the variable substrate, the concentration of CTP ($10K_m^{CTP}$) exceeded the K_i^{CTP}. The apparent value of k_{cat}^{MEP} ($^{app}k_{cat}^{MEP}$) was therefore lower than the corresponding $^{Obs}k_{cat}^{CTP}$ for all but YgbP mutants T140V and R109A. To allow direct comparison of k_{cat} values for each YgbP mutant, the initially determined $^{app}k_{cat}^{MEP}$ was corrected according to eq 3, which takes into account substrate inhibition by CTP. Notably, the corrected values of $^{Calc}k_{cat}^{MEP}$ for each mutant are in good agreement with the corresponding values of $^{Obs}k_{cat}^{CTP}$, as expected. Therefore, $^{Calc}k_{cat}^{MEP}$ was used to calculate the k_{cat}/K_m^{MEP} for MEP for each mutant. The values of the catalytic efficiency for CTP, k_{cat}/K_m^{CTP},

Table 1: Steady-State Kinetic Parameters for *E. coli* wt YgbP and Mutants

	MEP				CTP			
YgbP	K_m (mM)	$^{app}k_{cat}$[a] (s^{-1})	$^{Calc}k_{cat}$[a] (s^{-1})	k_{cat}/K_m (s^{-1} mM^{-1})	K_m (mM)	K_i (mM)	$^{Obs}k_{cat}$ (s^{-1})	k_{cat}/K_m (s^{-1} mM^{-1})
wt	0.37 ± 0.06	25.9 ± 5.9	48.4 ± 11.0	131	0.76 ± 0.06	19.6 ± 5.5	54.1 ± 28.0	71
T140V[b]	49.0 ± 7.3	2.7 ± 0.3	4.0 ± 0.4	0.08	2.0 ± 0.2	46.5 ± 6.6	1.8 ± 0.12[c]	0.9
R109A	131.5 ± 6.1	0.27 ± 0.07	0.4 ± 0.1	0.003	3.00 ± 0.02	68.9 ± 8.5	0.26 ± 0.03[c]	0.1
D106E	15.5 ± 4.5	0.54 ± 0.36	0.9 ± 0.6	0.06	1.4 ± 0.1	26.9 ± 1.5	0.93 ± 0.89	0.66
D106N	inactive							
D106A	inactive							
T165V	inactive							
K27S	3.0 ± 3.2	0.04 ± 0.01	0.75 ± 0.2	0.25	1.1 ± 0.3	12.3 ± 3.7	2.05 ± 0.32	0.5
K27A	inactive							
K213S	inactive							
R20K	0.31 ± 0.01	6.7 ± 1.6	21.4 ± 5.1	69	3.7 ± 0.8	7.2 ± 1.7	53.6 ± 1.5	14.5
R20A	3.28 ± 0.02	22.6 ± 0.7	52.7 ± 1.6	16	6.60 ± 0.03	16.2 ± 6.5	40.2 ± 9.6	6
R19K	0.74 ± 0.39	23.2 ± 2.4	47.2 ± 4.9	64	0.85 ± 0.17	14.2 ± 6.3	46.4 ± 14.8	54.6
R19A	2.98 ± 0.22	19.6 ± 3.6	36.8 ± 6.7	12	2.8 ± 1.1	20.5 ± 7.4	27.5 ± 2.8	10

[a] The $^{app}k_{cat}^{MEP}$ is the value of k_{cat}^{MEP} obtained by fitting the data to eq 1. $^{Calc}k_{cat}^{MEP}$ is the calculated value of k_{cat}^{MEP} after correction for the effects of substrate inhibition by CTP, using eq 3. [b] T104V displayed substrate inhibition by MEP (K_i^{MEP} = 100 ± 44 mM). [c] The $^{app}k_{cat}^{CTP}$ obtained from fitting the data to eq 2 was corrected using eq 4, taking into account that the fixed concentration of MEP was below saturation for each mutant, giving rise to $^{app}k_{cat}^{CTP}$ values of 1.21 ± 0.08 s^{-1} for T140V and 0.17 ± 0.02 s^{-1} for R109A.

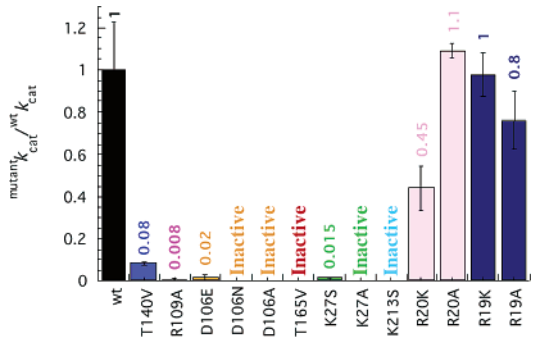

FIGURE 5: Relative k_{cat} values for YgbP mutants.

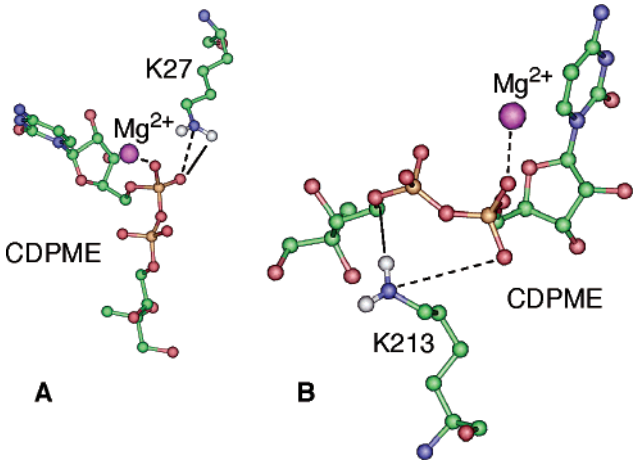

FIGURE 6: (A) Interaction of Lys27 of YgbP with CDPME. (B) Interaction of Lys213 of YgbP with CDPME. Dashed lines represent ionic interactions, and solid lines represent hydrogen bonds.

were calculated directly from $^{Obs}k_{cat}^{CTP}$ for all but YgbP mutants T140V and R109A. In the latter two cases, the elevated K_m^{MEP} and limited solubility of MEP required the use of concentrations of MEP close to K_m^{MEP}, resulting in values of $^{app}k_{cat}^{MEP}$ that were corrected using eq 4.

Although steady-state kinetic parameters could be determined for individual assay sets with high experimental precision (standard deviation for k_{cat} = ±1−3%, standard deviation for K_m = ±5−30%), separate kinetic runs on the same mutant showed a greater spread in final values, presumably due to variation in the activity of individual protein samples. The steady-state parameters reported in Table 1 therefore represent the average of two or more independent sets of assays, and the stated errors correspond to the standard deviation of each set of assays. The mechanism and biochemical significance, if there is any, of the observed substrate inhibition by CTP remain obscure. For purposes of this study, however, this inhibition was relevant only insofar as it required correction of the calculated parameters to allow meaningful, quantitative comparisons among the steady-state parameters for the various YgbP mutants. In the discussion below, only 2-fold or greater changes in individual steady-state kinetic parameters are considered to be mechanistically significant.

DISCUSSION

Stabilization of the Transition State for Cytidyl Transfer. Pulse−chase experiments are consistent with formation of the ternary YgbP·CTP·MEP complex by an ordered-sequential process in which CTP binds first. Figure 1 compares the conformation of bound substrate CTP with that of bound product CDPME. On the basis of the relative orientations of the scissile P−O bond of CTP and the newly formed P−O bond in the MEP-derived moiety of CDPME, it can be inferred that the cytidyltransferase reaction involves an in-line geometric relationship between the nucleophilic phosphate moiety of substrate MEP and the departing inorganic pyrophosphate. Figure 2 schematically illustrates the major interactions of the proposed pentacoordinate phosphate intermediate or transition state with the key active site residues of YgbP. As seen in Figures 1 and 6A, the α-phosphate oxygen atom of CTP and the cognate phosphate moiety of CDPME both interact with the ammonium group of the Lys27 side chain. There is also an ionic interaction between this same phosphate group and the ammonium group of Lys213, which in turn also appears to hydrogen bond to the bridging phosphate ester oxygen atom of CDPME (Figure 6B). Both the K213S and K27A mutations completely abolish YgbP activity, with <1.5% residual activity being observed for the corresponding K27S mutation (Table 1 and Figure 5). These results are consistent with the expected loss of stabilization of the pentacoordinate transition state or intermediate for the proposed in-line displacement mechanism.

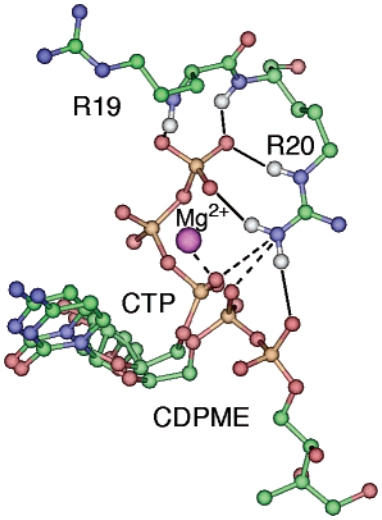

FIGURE 7: Interaction of Arg19 and Arg20 of YgbP with CTP and with CDPME. Dashed lines represent ionic interactions, and solid lines represent hydrogen bonds.

The δ-guanidino group of Arg20 interacts with substrate CTP through a combination of hydrogen bonds and ionic interactions with both the α- and γ-phosphate groups, as well as with both phosphate groups in the product, CDPME, one of which is derived from the α-phosphate of CTP and the other of which originates from the phosphate of MEP (Figure 7). Unexpectedly, neither the R20K mutant nor the less conservative R20A mutant showed significant reductions in k_{cat} compared to that of wt YgbP (Table 1 and Figure 5). The R20A mutant did exhibit modest 8−10-fold increases in K_m for both MEP and CTP, suggesting a reduced binding affinity for each substrate, but little differential change in the free energy of binding upon going from the ternary substrate complex to the bound pentacoordinate phosphate transition state. It is conceivable that, in the absence of Arg20, the Mg^{2+} cation, which interacts with the same nonbridging phosphate oxygen atom as does the side chain of Arg20, is alone sufficient for orienting and stabilizing both the ground state and the transition state for the cytidyltransferase reaction. Arg19 also appears to interact directly with the γ-phosphate of the CTP moiety through its backbone NH group and indirectly through its side chain via a water molecule. Not surprisingly, therefore, the conservative R19K mutation resulted in essentially no change in k_{cat} and relatively minor changes in k_{cat}/K_m (Table 1 and Figure 5). By contrast, the corresponding R19A mutant showed modest 7−10-fold reductions in k_{cat}/K_m for both substrates, largely due to increases in the corresponding values of K_m for both MEP and CTP, suggesting a possible change in the conformation of the free R19A mutant protein that is overcome by the binding of both substrates.

Binding and Reactivity of MEP. The interactions between active site residues and the MEP-derived portion of CDPME are evident from the X-ray structure of the YgbP·CDPME complex (*35*) (Figure 1). Since these interactions presumably also reflect the relationship between substrate MEP and the active site, the structure of the YgbP·CDPME complex can be used to explain the observed changes in the steady-state kinetic properties of YgbP mutants with respect to MEP.

As summarized schematically in Figures 1 and 2 and illustrated in Figure 8, active site residues Asp106, Arg109,

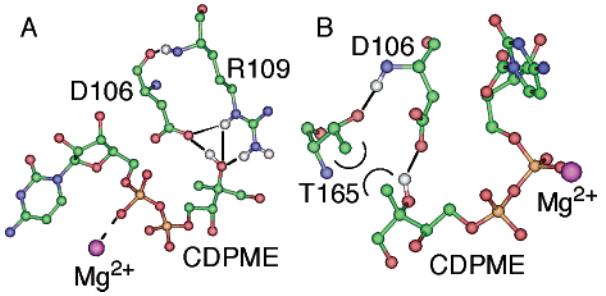

FIGURE 8: (A) Interaction of Asp106 and Arg109 of YgbP with the MEP-derived portion of CDPME. (B) Interaction of Asp106 and Thr165 of YgbP with the MEP-derived portion of CDPME. Dashed lines represent ionic interactions, and solid lines represent hydrogen bonds.

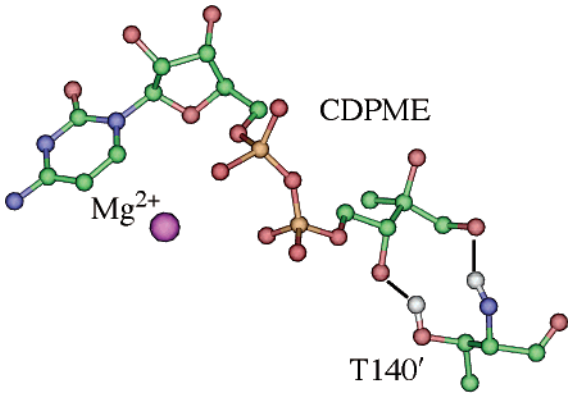

FIGURE 9: Interaction of Thr140′, derived from the paired subunit of the YgbP homodimer, with the MEP-derived portion of CDPME. Solid lines represent hydrogen bonds.

and Thr165 participate in a complex network of hydrogen bonds involving all three side chains as well as the peptide backbones of Arg109 and Asp106, resulting in a tridentate hydrogen bonding interaction of Asp106 and Arg109 with the 2-hydroxyl group of CDPME and, by extension, MEP. Consistent with this picture, the corresponding T165V, D106N, and D106A mutants are all completely inactive, while the D106E and R109A mutants display at most 2 and 0.8% of the k_{cat} of wt YgbP, respectively (Table 1 and Figure 5). Mutants D106E and R109A also suffer additional 40- and 350-fold increases, respectively, in the K_m for MEP, compared to that of wt YgbP, while the K_m values for CTP exhibit only relatively modest 2−4-fold increases for these two mutants. These effects are readily understood in terms of the ordered sequential mechanism, since the observed K_m for the initially bound CTP, which should be equal to the dissociation constant K_S, is unlikely to be affected significantly by perturbation of the binding or turnover of the second substrate MEP. The loss of activity observed for the T165V mutation may reflect loss of the H-bond to the Asp106 backbone NH group as well as loss of the hydrophobic packing interaction of the side chain methyl with the 2C-methyl of the MEP substrate (Figure 8B). In this light, it is interesting that the substrate analogue erythritol 4-phosphate, which lacks the 2C-methyl group of MEP, is both a modest inhibitor and poor substrate for wt YgbP.

The side chain hydroxyl and backbone NH group of Thr140′, contributed by the paired subunit of the YgbP homodimer, are hydrogen bonded to the C-3 and C-1 hydroxyl oxygen atoms, respectively, of the MEP-derived portion of CDPME (Figure 9). Thr140′ does not interact

directly with CTP, since in the YgbP•CTP complex, Thr140′ and CTP are separated by at least 12 Å. In the T140V mutant, the k_{cat} is decreased to 8% of that of wt YgbP, while k_{cat}/K_m for MEP has been decreased more than 1600-fold, due to an additional 130-fold increase in the corresponding K_m for MEP (Table 1). Not surprisingly, the T140V mutation results in an only modest 2-fold increase in the K_m for CTP.

CONCLUSIONS

Taken together, these results firmly establish the importance of YgbP residues Asp106, Arg109, Thr165, and Thr140′ in binding MEP in an interlocking network of hydrogen bonds and van der Waals packing interactions, thereby precisely positioning the MEP substrate for nucleophilic attack on the α-phosphate of the prebound cosubstrate CTP. As previously suggested (*35*), Arg157 is also likely to play a role by positioning the nucleophilic phosphate residue of MEP near the α-phosphate of CTP, but we have not yet examined this possibility experimentally. Lys213 can draw the nucleophilic and electrophilic phosphate groups together through a combination of hydrogen bonds and ionic interactions and, along with Lys27, balance the negative charge on the target α-phosphate of the CTP while also stabilizing the developing negative charge on the pentacoordinate phosphate intermediate. At the same time, the divalent Mg^{2+} cation assists in neutralizing the developing negative charge in the pentacoordinate phosphate intermediate and then facilitates the departure of the pyrophosphate group during the subsequent collapse of this intermediate. Surprisingly, neither the apparent contribution of Arg20 to the stabilization of the pentacoordinate phosphate, the interaction of Arg20 with the γ-phosphate of CTP, nor hydrogen bonding of Arg20 to the nucleophilic phosphate of MEP appears to be critical to the k_{cat} for the cytidyltransferase reaction. On the other hand, replacement of Arg20 with Ala does result in a minor, 8−10-fold reduction in k_{cat}/K_m for both CTP and MEP, presumably due to changes in the conformation of the free enzyme, with consequent increases in the corresponding K_m values for each substrate, while replacment of Arg20 with Lys results in a similar 12-fold decrease in k_{cat}/K_m for CTP, but no significant change in k_{cat}/K_m for MEP.

REFERENCES

1. Rohmer, M. (1999) A Mevalonate-Independent Route to Isopentenyl Diphosphate, in *Comprehensive Natural Products Chemistry. Isoprenoids Including Carotenoids and Steroids* (Cane, D. E., Ed.) pp 45−67, Elsevier, Oxford, U.K.
2. Rohmer, M. (1999) The discovery of a mevalonate-independent pathway for isoprenoid biosynthesis in bacteria, algae and higher plants, *Nat. Prod. Rep. 16*, 565−574.
3. Schwarz, M., and Arigoni, D. (1999) Gingkolide Biosynthesis, in *Comprehensive Natural Products Chemistry. Isoprenoids Including Carotenoids and Steroids* (Cane, D. E., Ed.) pp 367−400, Elsevier, Oxford, U.K.
4. Kawasaki, T., Kuzuyama, T., Furihata, K., Itoh, N., Seto, H., and Dairi, T. (2003) A relationship between the mevalonate pathway and isoprenoid production in actinomycetes, *J. Antibiot. 56*, 957−966.
5. Eisenreich, W., Rohdich, F., and Bacher, A. (2001) Deoxyxylulose phosphate pathway to terpenoids, *Trends Plant Sci. 6*, 78−84.
6. Rohdich, F., Kis, K., Bacher, A., and Eisenreich, W. (2001) The non-mevalonate pathway of isoprenoids: genes, enzymes and intermediates, *Curr. Opin. Chem. Biol. 5*, 535−540.
7. Kuzuyama, T., and Seto, H. (2003) Diversity of the biosynthesis of the isoprene units, *Nat. Prod. Rep. 20*, 171−183.
8. Kuzuyama, T., Takahashi, S., Watanabe, H., and Seto, H. (1998) Direct Formation of 2-*C*-Methyl-D-Erythritol 4-Phosphate from 1-Deoxy-D-Xylulose 5-Phosphate by 1-Deoxy-D-Xylulose 5-Phosphate Reductoisomerase, A New Enzyme in the Non-Mevalonate pathway to Isopentenyl Diphosphate, *Tetrahedron Lett. 39*, 4509−4512.
9. Sprenger, G. A., Schörken, U., Wiegert, T., Grolle, S., De Graaf, A. A., Taylor, S. V., Begley, T. P., Bringer-Meyer, S., and Sahm, H. (1997) Identification of a thiamin-dependent synthase in *Escherichia coli* required for the formation of the 1-deoxy-D-xylulose 5-phosphate precursor to isoprenoids, thiamin, and pyridoxol, *Proc. Natl. Acad. Sci. U.S.A. 94*, 12857−12862.
10. Lois, L. M., Campos, N., Putra, S. R., Danielsen, K., Rohmer, M., and Boronat, A. (1998) Cloning and characterization of a gene from *Escherichia coli* encoding a transketolase-like enzyme that catalyzes the synthesis of D-1-deoxyxylulose 5-phosphate, a common precursor for isoprenoid, thiamin, and pyridoxol biosynthesis, *Proc. Natl. Acad. Sci. U.S.A. 95*, 2105−2110.
11. David, S., Estramareix, B., Fischer, J. C., and Therisod, M. (1981) 1-Deoxy-D-threo-2-pentulose: the precursor of the five-carbon chain of the thiazole of thiamine, *J. Am. Chem. Soc. 103*, 7341−7342.
12. Himmeldirk, K., Sayer, B. G., and Spenser, I. D. (1998) Comparative Biogenetic Anatomy of Vitamin B_1: A ^{13}C NMR Investigation of the Biosynthesis of Thiamin in *Escherichia coli* and in *Saccharomyces cerevisiae*, *J. Am. Chem. Soc. 120*, 3581−3589.
13. Hill, R. E., Himmeldirk, K., Kennedy, I. A., Pauloski, R. M., Sayer, B. G., Wolf, E., and Spenser, I. D. (1996) The biogenetic anatomy of vitamin B_6. A ^{13}C NMR investigation of the biosynthesis of pyridoxol in *Escherichia coli*, *J. Biol. Chem. 271*, 30426−30435.
14. Cane, D. E., Du, S., Robinson, J. K., Hsiung, Y.-J., and Spenser, I. D. (1999) Biosynthesis of Vitamin B_6. Enzymatic Conversion of 1-Deoxy-D-xylulose-5-phosphate to Pyridoxol Phosphate, *J. Am. Chem. Soc. 121*, 7722−7723.
15. Rohdich, F., Wungsintaweekul, J., Fellermeier, M., Sagner, S., Herz, S., Kis, K., Eisenreich, W., Bacher, A., and Zenk, M. H. (1999) Cytidine 5′-triphosphate-dependent biosynthesis of isoprenoids: YgbP protein of *Escherichia coli* catalyzes the formation of 4-diphosphocytidyl-2-C-methylerythritol, *Proc. Natl. Acad. Sci. U.S.A. 96*, 11758−11763.
16. Kuzuyama, T., Takagi, M., Kaneda, K., Tohru, and Seto, H. (2000) Formation of 4-(cytidine 5′-diphospho)-2-C-methyl-D-erythritol from 2-C-methyl-D-erythritol 4-phosphate by 2-C-methyl-D-erythritol 4-phosphate cytidylyltransferase, a new enzyme in the nonmevalonate pathway, *Tetrahedron Lett. 41*, 703−706.
17. Kuzuyama, T., Takagi, M., Kaneda, K., Watanabe, H., Dairi, T., and Seto, H. (2000) Studies on the nonmevalonate pathway: conversion of 4-(cytidine 5′-diphospho)-2-C-methyl-D-erythritol to its 2-phospho derivative by 4-(cytidine 5′-diphospho)-2-C-methyl-D-erythritol kinase, *Tetrahedron Lett. 41*, 2925−2928.
18. Luttgen, H., Rohdich, F., Herz, S., Wungsintaweekul, J., Hecht, S., Schuhr, C. A., Fellermeier, M., Sagner, S., Zenk, M. H., Bacher, A., and Eisenreich, W. (2000) Biosynthesis of terpenoids: YchB protein of *Escherichia coli* phosphorylates the 2-hydroxy group of 4-diphosphocytidyl-2C-methyl-D-erythritol, *Proc. Natl. Acad. Sci. U.S.A. 97*, 1062−1067.
19. Herz, S., Wungsintaweekul, J., Schuhr, C. A., Hecht, S., Luttgen, H., Sagner, S., Fellermeier, M., Eisenreich, W., Zenk, M. H., Bacher, A., and Rohdich, F. (2000) Biosynthesis of terpenoids: YgbB protein converts 4-diphosphocytidyl-2C-methyl-D-erythritol 2-phosphate to 2C-methyl-D-erythritol 2,4-cyclodiphosphate, *Proc. Natl. Acad. Sci. U.S.A. 97*, 2486−2490.
20. Takagi, M., Kuzuyama, T., Kaneda, K., Watanabe, H., Dairi, T., and Seto, H. (2000) Studies on the nonmevalonate pathway: formation of 2-C-methyl-D-erythritol 2,4-cyclodiphosphate from 2-phospho-4-(cytidine 5′-diphospho)-2-C-methyl-D-erythritol, *Tetrahedron Lett. 41*, 3395−3398.
21. Hecht, S., Eisenreich, W., Adam, P., Amslinger, S., Kis, K., Bacher, A., Arigoni, D., and Rohdich, F. (2001) Studies on the nonmevalonate pathway to terpenes: the role of the GcpE (IspG) protein, *Proc. Natl. Acad. Sci. U.S.A. 98*, 14837−14842.
22. Seemann, M., Campos, N., Rodriguez-Concepcion, M., Ibanez, E., Duvold, T., Tritsch, D., Boronat, A., and Rohmer, M. (2002) Isoprenoid biosynthesis in *Escherichia coli* via the methylerythritol phosphate pathway: enzymatic conversion of methylerythritol cyclodiphosphate into a phosphorylated derivative of (*E*)-2-methylbut-2-ene-1,4-diol, *Tetrahedron Lett. 43*, 1413−1415.
23. Altincicek, B., Kollas, A. K., Sanderbrand, S., Wiesner, J., Hintz, M., Beck, E., and Jomaa, H. (2001) GcpE is involved in the 2-C-

methyl-D-erythritol 4-phosphate pathway of isoprenoid biosynthesis in *Escherichia coli*, *J. Bacteriol. 183*, 2411−2416.
24. Cunningham, F. X., Jr., Lafond, T. P., and Gantt, E. (2000) Evidence of a role for LytB in the nonmevalonate pathway of isoprenoid biosynthesis, *J. Bacteriol. 182*, 5841−5848.
25. Altincicek, B., Kollas, A., Eberl, M., Wiesner, J., Sanderbrand, S., Hintz, M., Beck, E., and Jomaa, H. (2001) LytB, a novel gene of the 2-C-methyl-D-erythritol 4-phosphate pathway of isoprenoid biosynthesis in *Escherichia coli*, *FEBS Lett. 499*, 37−40.
26. Rohdich, F., Hecht, S., Gartner, K., Adam, P., Krieger, C., Amslinger, S., Arigoni, D., Bacher, A., and Eisenreich, W. (2002) Studies on the nonmevalonate terpene biosynthetic pathway: Metabolic role of IspH (LytB) protein, *Proc. Natl. Acad. Sci. U.S.A. 99*, 1158−1163.
27. Rohdich, F., Zepeck, F., Adam, P., Hecht, S., Kaiser, J., Laupitz, R., Grawert, T., Amslinger, S., Eisenreich, W., Bacher, A., and Arigoni, D. (2003) The deoxyxylulose phosphate pathway of isoprenoid biosynthesis: Studies on the mechanisms of the reactions catalyzed by IspG and IspH protein, *Proc. Natl. Acad. Sci. U.S.A. 100*, 1586−1591.
28. Seemann, M., Bui, B. T. S., Wolff, M., Tritsch, D., Campos, N., Boronat, A., Marquet, A., and Rohmer, M. (2002) Isoprenoid biosynthesis through the methylerythritol phosphate pathway: the (*E*)-4-hydroxy-3-methylbut-2-enyl diphosphate synthase (GcpE) is a [4Fe-4S] protein, *Angew. Chem., Int. Ed. 41*, 4337−4339.
29. Kuzuyama, T., Shimizu, T., Takahashi, S., and Seto, H. (1998) Fosmidomycin, a Specific Inhibitor of 1-Deoxy-D-Xylulose 5-Phosphate Reductoisomerase in the Nonmevalonate Pathway for Terpenoid Biosynthesis, *Tetrahedron Lett. 39*, 7913−7916.
30. Hintz, M., Reichenberg, A., Altincicek, B., Bahr, U., Gschwind, R. M., Kollas, A. K., Beck, E., Wiesner, J., Eberl, M., and Jomaa, H. (2001) Identification of (*E*)-4-hydroxy-3-methyl-but-2-enyl pyrophosphate as a major activator for human $\gamma\delta$ T cells in *Escherichia coli*, *FEBS Lett. 509*, 317−322.
31. Jomaa, H., Wiesner, J., Sanderbrand, S., Altincicek, B., Weidemeyer, C., Hintz, M., Turbachova, I., Eberl, M., Zeidler, J., Lichtenthaler, H. K., Soldati, D., and Beck, E. (1999) Inhibitors of the nonmevalonate pathway of isoprenoid biosynthesis as antimalarial drugs, *Science 285*, 1573−1576.
32. Wungsintaweekul, J. (2001) Ph.D. Thesis, Technische Universitaet Muenchen, Munich, Germany.
33. Cane, D. E., Chow, C., Lillo, A., and Kang, I. (2001) Molecular cloning, expression and characterization of the first three genes in the mevalonate-independent isoprenoid pathway in *Streptomyces coelicolor*, *Bioorg. Med. Chem. 9*, 1467−1477.
34. Lillo, A. M., Tetzlaff, C. N., Sangari, F. J., and Cane, D. E. (2003) Functional expression and characterization of EryA, the erythritol kinase of *Brucella abortus*, and enzymatic synthesis of L-erythritol-4-phosphate, *Bioorg. Med. Chem. Lett. 13*, 737−739.
35. Richard, S. B., Bowman, M. E., Kwiatkowski, W., Kang, I., Chow, C., Lillo, A. M., Cane, D. E., and Noel, J. P. (2001) Structure of 4-diphosphocytidyl-2-C-methylerythritol synthetase involved in mevalonate-independent isoprenoid biosynthesis, *Nat. Struct. Biol. 8*, 641−648.
36. Kemp, L. E., Bond, C. S., and Hunter, W. N. (2003) Structure of a tetragonal crystal form of *Escherichia coli* 2C-methyl-D-erythritol 4-phosphate cytidylyltransferase, *Acta Crystallogr. 59*, 607−610.
37. Jez, J. M., Ferrer, J. L., Bowman, M. E., Dixon, R. A., and Noel, J. P. (2000) Dissection of malonyl-coenzyme A decarboxylation from polyketide formation in the reaction mechanism of a plant polyketide synthase, *Biochemistry 39*, 890−902.
38. Sambrook, J., Fritsch, E. F., and Maniatis, T. (1989) *Molecular Cloning, A Laboratory Manual*, 2nd ed., Cold Spring Harbor Laboratory Press, Plainview, NY.
39. Bradford, M. (1976) A Rapid and Sensitive Method for the Quantitation of Microgram Quantitites of Protein Utilizing the Principle of Protein-Dye Binding, *Anal. Biochem. 72*, 248−254.
40. Jones, T. A., and Kjeldgaard, M. (1997) Electron-density map interpretation, *Methods Enzymol. 277*, 173−208.
41. Kraulis, P. J. (1991) MOLSCRIPT: a program to produce both detailed and schematic plots of protein structures, *J. Appl. Crystallogr. 24*, 945−949.
42. Rose, I. A. (1980) The Isotope Trapping Method: Desorption Rates of Productive E·S Complexes, *Methods Enzymol. 64*, 47−59.
43. Fersht, A. R. (1985) Basic equations of enzyme kinetics, in *Enzyme structure and mechanism*, pp 114, W. H. Freeman and Co., New York.

BI0487241